Revisiting the Storage Capacity Limit of Graphite Battery Anodes: Spontaneous Lithium Overintercalation at Ambient Pressure

Cristina Grosu,[1,2] Chiara Panosetti,[3,*] Steffen Merz,[1] Peter Jakes,[1] Stefan Seidlmayer,[4] Sebastian Matera,[3,5] Rüdiger-A. Eichel,[1,6] Josef Granwehr,[1,7] and Christoph Scheurer[3,†]

[1] *Institute of Energy and Climate Research (IEK-9), Forschungszentrum Jülich, Jülich 52425, Germany*

[2] *Chair for Theoretical Chemistry and Catalysis Research Center, Technical University of Munich, Garching 85747, Germany*

[3] *Fritz-Haber-Institut der Max-Planck-Gesellschaft, Berlin 14195, Germany*

[4] *Heinz Maier-Leibnitz Zentrum (MLZ), Technische Universität München, Garching b. München, Germany*

[5] *Institute for Mathematics, Freie Universität Berlin, Berlin 14195, Germany*

[6] *RWTH Aachen University, Institute of Physical Chemistry, Aachen D-52074, Germany*

[7] *RWTH Aachen University, Institute of Technical and Macromolecular Chemistry, Aachen D-52074, Germany*

(Received 15 November 2021; revised 13 January 2023; accepted 20 January 2023; published 1 March 2023)

The market quest for fast-charging, safe, long-lasting, and performant batteries drives the exploration of new energy storage materials, but also promotes fundamental investigations of materials already widely used. Presently, renewed interest in anode materials is observed—primarily graphite electrodes for lithium-ion batteries. Here, we focus on the upper limit of lithium intercalation in the morphologically quasi-ideal highly oriented pyrolytic graphite, with a LiC_6 stoichiometry corresponding to nominally 100% state of charge. We prepare a sample by immersion in liquid lithium at ambient pressure and investigate it by static ^{7}Li nuclear magnetic resonance (NMR). We resolve unexpected signatures of superdense intercalation compounds, LiC_{6-x}. These have been ruled out for decades, since the highest geometrically accessible composition, LiC_2, can only be prepared under high pressure. We thus challenge the widespread notion that any additional intercalation beyond LiC_6 is insignificant under ambient conditions. We monitor the sample upon calendaric ageing and employ *ab initio* calculations to rationalize the NMR results. Computed relative stabilities of different superdense configurations reveal that non-negligible overintercalation does proceed spontaneously beyond the currently accepted capacity limit. The associated capacity gain is not worth pushing graphitic battery anodes beyond the LiC_6 limit in practical applications; rather these findings carry more fundamental implications. Neglecting overintercalation may hinder the correct interpretation of experimental observations, as well as the correct design of computational models, in investigations of performance-critical phenomena, as it is likely to play a crucial role in the onset mechanism of lithium plating and dendrite formation in real battery materials.

DOI: 10.1103/PRXEnergy.2.013003

I. INTRODUCTION

Mass market penetration of electric vehicles is a key element to achieve a nearly CO_2-free transportation sector [1]. Powerful, durable, and safe lithium-ion batteries (LIBs) are crucial for consumer acceptance of electromobility on a larger scale. In particular, the fast-charging capability is regarded as a pivotal selling point. The necessity of fast-charging batteries brought some intrinsic limitations of the materials back into the spotlight, which historically did not matter in commonplace applications of LIBs, such as portable electronics [2]. Primarily for the negative electrode, notable issues are still largely unaddressed to this day, including increasing the active site density, earlier detection of dendrite formation, or a quantitative description of mass and charge transport [3–6]. An extensive amount of work is ongoing to identify alternatives to the carbon-based anode materials [7]. Even within the class of carbonaceous materials, different options were screened for usage as negative electrodes, from soft to hard carbon, carbon foam, carbon

*panosetti@fhi.mpg.de
†scheurer@fhi.mpg.de

nanotubes, graphene sheets, artificial graphite, or mesocarbon microbeads graphite (MCMB) [8].

Nonetheless, with its intrinsic capacity and wide availability, graphite is still the most employed anode material. Its working principle is based on the intercalation of lithium ions. Upon electrochemical lithium intercalation during charging, graphite reaches its maximum reversible Li storage capacity at a lithium-to-carbon ratio of 1:6 (LiC_6). Theoretically, this compound yields a capacity of 372 mAh/g, commonly defining 100% state of charge (SOC) [8–10]. However, the highest geometrically accessible composition—not considering lithium carbide (Li_2C_2) but only the family of graphite intercalation compounds (GICs)—is not LiC_6, but LiC_2, with a capacity 3 times higher. However, the latter is metastable at ambient conditions and its nonelectrochemical preparation was only reported under high pressure, with superdense decomposition products, LiC_{6-x} with $x > 0$, stable over an extended time period [11,12].

Despite extensive experimental efforts, in-depth understanding of *in operando* battery processes is still incomplete [13–16]. One major problem is that the interconnection of many relevant electrochemical processes renders the analysis of experimental data difficult and complicates the understanding of actual limits and causes of battery cell failure [5]. Furthermore, theoretical investigations over large compositional Li:C ratios, and on time scales relevant for Li dynamics in graphite without unrealistic simplifications have only become possible recently. Therefore, concomitant theoretical and experimental research is scarce.

One particularly problematic aspect is the very large scatter in reported values for diffusion coefficients of lithium ions in graphitic hosts, ranging from approximately 4×10^{-6} cm^2/s [17] to approximately 8×10^{-11} cm^2/s [18] for in-plane motion (see, e.g., Ref. [8]).

Here, we use highly oriented pyrolytic graphite (HOPG) as a model system to investigate lithium ion intercalation, providing nuclear-magnetic-resonance (NMR) reference data from a system as well defined as possible for further *in operando* studies of the lithium diffusion dynamics in LIBs. To exclude any external influence on the intercalation process, we opt for an infiltration technique under ambient pressure [19–21]. Figure 1 shows a sketch of the synthesis workflow, using lithium metal and HOPG as precursors. More details on the preparation are provided in Sec. II and in the Supplemental Material [22] [see Figs. S1(a) and S1(b)]. Using this slow intercalation route, we obtain a sample that, repeatedly analyzed in detail, showed unexpected spectroscopic evidence of superdense structures. We assess the plausibility of such an assignment of spectral features by *ab initio* calculations. Eventually, we analyze the long-term evolution of the sample over several months, concluded by heating it up to 60 °C.

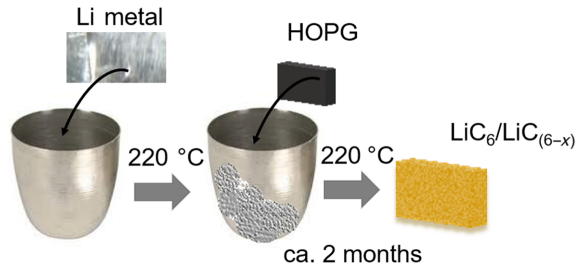

FIG. 1. Schematic representation of the conducted synthesis. First, metallic lithium is melted and kept at 220 °C. Subsequently, a HOPG sample with dimensions $10.0 \times (4.9) \times 2.0$ mm^3 is added. Tweezers are used to keep the HOPG in contact with molten lithium for a few minutes to start the intercalation. The system is then held for approximately ten weeks at constant conditions to ensure full intercalation into the HOPG.

A. What do we know about superdense LiC_2 and LiC_{6-x}?

Superdense realizations of lithium GICs were reported at high pressure and temperature conditions since the 1980s [11,23–29]. Figure 2 schematically shows possible high-symmetry structures for some intermediate stoichiometries between LiC_6 and LiC_2.

The occurrence of LiC_2 was excluded *a priori* from any working battery for a long time. Since its nonelectrochemical synthesis was always performed at high pressure and temperature, it is considered unlikely to be found in secondary batteries [12,24,30]. Alternatively to high-pressure synthesis, ball milling also allows LiC_2 to be prepared using artificial graphite, MCMB, and carbon foam [28,30,31]. However, one may argue that ball milling produces high pressure and temperature locally [32]. Once the pressure is released, the LiC_2 composition becomes unstable and approaches $LiC_{2.2-2.7,3.4}$ [24,33]. Nevertheless, $LiC_{2.7}$ and $LiC_{3.4}$ as decomposition products of LiC_2 were reported to be stable enough to allow measurements at ambient conditions [25,26]. Bindra *et al.* [25] stabilized superdense GICs using boron doping, in an attempt to enable higher capacity electrode materials, yet they still used high-pressure synthesis.

For electrochemical intercalation, Conard *et al.* [34] reported that the electric field actuates only as far as the gallery entrance, and therefore is not sufficiently attractive to drive the intercalation up to LiC_2. Notwithstanding, superdense phases were observed for electrochemical systems using different carbon-based matrices, leading to the concept of overcharged LIBs [35–37]. In the latter works, lithium ions appeared to continue intercalating after LiC_6 was formally reached, yet before being plated as lithium metal. Unfortunately, such overcharged anodes show irreversible capacity loss after the first deintercalation cycle [36]. More recently Paronyan *et al.* [38] successfully used carbon foam as anode material to investigate overlithiation.

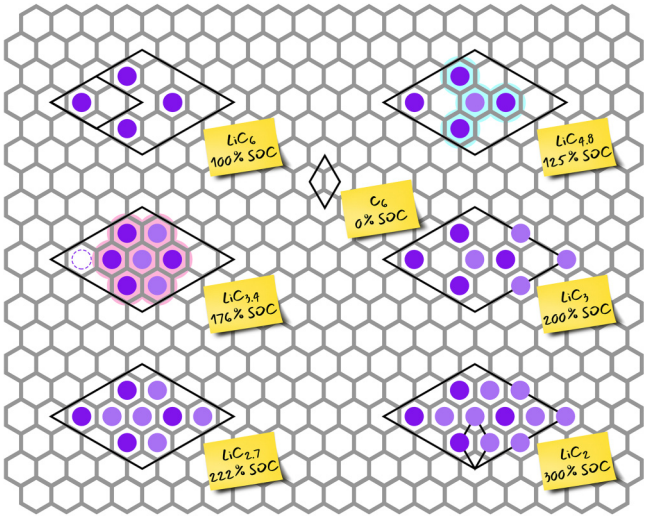

FIG. 2. Schematic single-layer representation of some superdense LiC_{6-x} high-symmetry structural motifs and respective (local) states of charge relative to LiC_6. The gray honeycomb represents the graphitic host lattice assumed to be AA stacked, and purple circles represent lithium atoms. Excess lithium with respect to LiC_6 is represented in lighter purple. The dotted circle in $LiC_{3.4}$ marks how at least one Li atom must move from its original position in order to achieve the Li_7 cluster motif. Black diamonds represent the smallest supercell commensurate to all the lithiated stoichiometries. For LiC_6 and LiC_2, the (smaller) primitive cell is also shown. Highlighted in red and cyan (for clarity, only shown in $LiC_{4.8}$ and $LiC_{3.4}$) are structural motifs that can give rise to high-ppm NMR signals, which appear as soon as any additional Li is inserted, and are recurring in any stoichiometry beyond LiC_6.

A systematic investigation of the relative stability of overlithiated compounds, especially the intermediate stoichiometries between LiC_6 and LiC_2, is currently missing, both from the experimental and the computational standpoints. On the experimental side, there is widespread consensus [39–42] that the free energy of intercalation of LiC_6 falls in the range of −6 to −14 kJ/mol (−0.06 to −0.14 eV). Yet little is known about the free energies of overintercalation, except that the formation of LiC_2 is assumed endergonic at ambient conditions. On the computational side, previous studies based on density functional theory (DFT) only report total energy calculations of LiC_6 and—less often—LiC_2 [12,43–45]. Two main limitations are recurring among these. First, dispersion interactions, which are crucial in intercalation chemistry, were not included in all the studies. Second, total energies only provide a "virtual" zero-temperature picture, while finite temperature and pressure require a description in terms of free energies. Despite these limitations, the reported total energies are compatible with the measured thermochemistry. However, no coherent body of literature exists that addresses the energetics of the entire LiC_{6-x} range on the same footing.

II. MATERIALS AND METHODS

A. Experiment

1. Synthesis and sample preparation

The LiC_6 sample is prepared using an infiltration technique. Metallic lithium with 99.9% purity (Sigma-Aldrich) is intercalated into highly oriented pyrolytic graphite HOPG (Goodfellow purchased by Sigma-Aldrich). The lithium metal is heated after the melting point up to 220 °C. The lithium's self-cleaning properties ensure a higher purity of the molten lithium metal. Afterwards the HOPG is added. In order to ensure complete lithium intercalation, the intercalation process is allowed to take place for a period of over 2 months. This long infiltration time is necessary due to the dimension of the host material [preintercalation size of $10.0 \times (4.9) \times 2.0\ mm^3$] [19–21]. The ageing process is performed in a closed container in a glove box under argon atmosphere. The sample is left to age for 5 months initially, followed by an additional period of 2 months. For the 5-month aged sample, a series of temperature dependency spectra of ^{7}Li static NMR are recorded.

2. NMR measurements and data analysis

All ^{7}Li NMR spectra are acquired using a Bruker BioSpin spectrometer Avance III HD 600 MHz XWB at $B_0 = 14.1$ T (^{7}Li Larmor frequency of 233.3 MHz), equipped with a Bruker DiffBB 5-mm BBO-H/F-Z gradient diffusion probe. A single 90° pulse excitation of 11 μs with recovery delays of 10 s on ^{7}Li is employed. The raw data are analyzed using MATLAB®. An exponential window function is employed before a fast Fourier transform. The spectra are zero- and first-order phase corrected as well as background corrected.

B. Computation

1. DFT calculations and ab initio thermodynamics

All the DFT calculations are performed using the plane-wave code VASP [47] v.5.4.4, with the Perdew-Burke-Ernzerhof functional [48] and the projector augmented-wave pseudopotentials [49]. Dispersion interactions are taken into account with the D3 method [50]. To ensure well-converged total energies, a basis-set cutoff of 599 eV is chosen. All the calculated geometries are represented in appropriate periodic supercells and the Brillouin zone is sampled at a fixed k-point density of 0.1 $Å^{-1}$. The vibrational densities of states are calculated using PHONOPY [51] at the harmonic approximation level. The chemical potential of lithium is mapped to a temperature in the 0–600 K range using JANAF thermochemical tables [52] up to the fusion temperature (453.69 K) and employing a linear approximation for higher temperatures (cf. Sec. 2 within the Supplemental Material [22]). *Ab initio*

molecular dynamics simulations are performed by means of the density-functional tight-binding (DFTB) [53] code DFTB+ [54] v.19.1 using the parametrization developed in our group [55,56]. Trajectories of variable length are propagated with a time step of 1 fs in the canonical ensemble at 500, 750, and 1000 K, using a Nosé-Hoover thermostat [57] with a coupling strength of 41 THz, corresponding to the highest vibrational mode of LiC_6 as calculated with PHONOPY.

III. RESULTS AND DISCUSSION

A. Static ^{7}Li NMR of the lithium-intercalated HOPG sample after preparation

Static ^{7}Li NMR spectroscopy is a valuable tool to distinguish different degrees of lithiation in carbonaceous materials [13]. The ^{7}Li nucleus possesses spin 3/2, making observations of central transitions and quadrupolar satellite transitions possible. Satellite transitions allow conclusions on ordered structures with low Li-ion mobility [20,34], whereas their absence may indicate a lack of perfectly ordered motifs and/or a motional averaging of the quadrupolar interaction [34].

Figure 3(a) shows a photograph of the fully intercalated HOPG sample. The golden color is characteristic of LiC_6. However, overlithiated compounds were also reported to appear golden [25,30]. Figure 3(b) represents the static ^{7}Li solid-state NMR spectrum of the polished sample. All chemical shifts are reported against an external reference of a 1.0-M solution of LiCl in D_2O. We assign the isotropic chemical shift at 45 parts per million (ppm) with quadrupolar satellites to LiC_6, compatibly with previous works [15,58,59]. Additionally, an asymmetric signal with a sharp peak at 274 ppm and a shoulder at approximately 256 ppm is present. We also observe a broad spectral feature around 100–200 ppm that is not background distortion (cf. Sec. 1 within the Supplemental Material [22]). At first, the high-ppm signals may be attributed to plated lithium on the sample. Signals in this ppm region are consistently present in all NMR experiments at the upper limit of lithium capacity, regardless of the specific form of carbonaceous host material [14,15,34,35,37,60,61]. For comparison, we also prepare a sample using graphite powder, mechanically intercalated using pestle and mortar in excess lithium, and we observe a similar signature (see Sec. I.B. within the Supplemental Material [22]).

The HOPG surface is polished using sand paper [see Supplementary Figs. S1(c) and S1(d) [22]], but residual metallic Li may persist. However, the intensity of the high-ppm ^{7}Li NMR signal is too high for only trace amounts of lithium metal on the surface that are not detectable by visual inspection. Moreover, HOPG can be considered a defect-free single crystal, thus lacking internal pores that could accommodate pockets of metallic lithium [62].

At this point, the possibility for these high-ppm signatures to be generated by superdense phases must be considered. Superdense Li GICs have not been reported without harsh pressure conditions. However, the uncertainty raised in our sample reflects the ambiguity of assignments present in the literature. Azaïs *et al.* [37] assigned a 259-ppm ^{7}Li NMR resonance to lithium metal, despite using the exact ratio of Li/C to form LiC_2 with a ball-milling synthesis. Interestingly, they found no Li metal signal in the x-ray

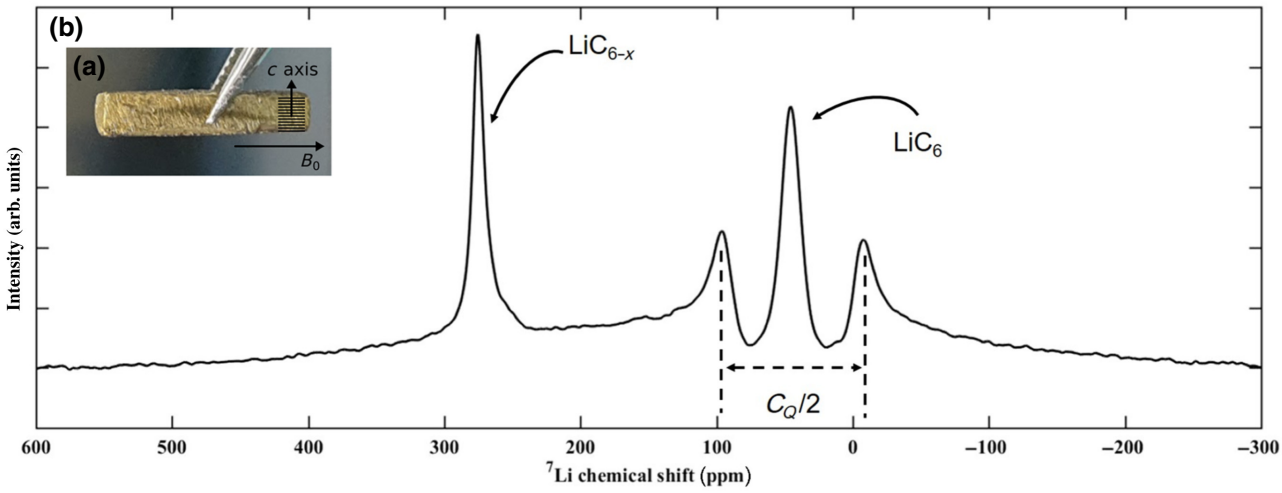

FIG. 3. Static ^{7}Li NMR and initial sample in the NMR tube. Inset (a) shows the golden color of lithium-intercalated HOPG, nominally corresponding to LiC_6 [9,20]. Schematics in overlay show the orientation of the graphite layers, the crystallographic *c* axis, and the direction of B_0. (b) Static ^{7}Li spectrum of lithium intercalated in HOPG. The isotropic chemical shift at 45 ppm is assigned to LiC_6. The quadrupolar satellites are compatible with a single-crystal pattern [20,34] (see Sec. I.C. within the Supplemental Material [22] for a brief discussion on quadrupolar satellites, which includes Ref. [46]). The quadrupolar coupling constant C_Q for LiC_6 is 46 kHz. The peak at 274 ppm and the shoulder at 256 ppm show the presence of superdense LiC_{6-x} compositions [28].

spectrum, which is explained by intensive milling applied to the sample. Conversely, Conard *et al.* [11] assigned a peak at 259 ppm to LiC_2. Since the spectrum is recorded after releasing the pressure, the stoichiometry of the GIC may not be LiC_2 anymore, and the true LiC_2 chemical shift might be closer to the Li metal shift. The observed 259-ppm peak, on the other hand, could alternatively be attributed to $LiC_{2.2-2.4}$ [11,24,33].

As shown in Fig. 2, two local structural motifs are recurring in superdense compositions: a Li_4 pattern in the shape of a three-pronged "star" (highlighted in cyan) and a denser Li_7 pattern in the shape of a flat cluster, or "flower" (highlighted in red). The central Li atom is coordinated by three or six nearest Li neighbors, respectively. It is therefore expected to exhibit pseudometallic character. This was already suggested to explain the high-ppm signals associated with LiC_2 decomposition products [24,30,34].

Chang *et al.* [61] showed that variable shifts at high ppm can arise from different microstructures of lithium metal in electrochemical systems. Since no current or potential is applied during sample preparation, the formation of dendrites or mossy-type microstructures is not expected here. Trease *et al.* [63] showed that lithium metal in nonspherical shapes is also sensitive to the direction of the magnetic field, with resonances shifting between about 245 and 270 ppm if a planar sample is placed perpendicular or parallel to B_0, respectively. This is known as orientation-dependent shift due to the bulk magnetic susceptibility effect. All our comparative measurements are performed using the same sample orientation, with the *c* axis perpendicular to B_0 (Fig. 3). In a control experiment, we also cut part of the sample to measure at parallel orientation. The high-ppm signature only moved to 264 ppm (Supplementary Fig. S3 [22]) within the limits set by the original 274 and 256 ppm signals. This also indicates a susceptibility effect for the quasimetallic superdense species, as has previously been observed for Li metal.

B. Calendar ageing and postageing temperature-dependent static ^{7}Li NMR

We age the sample to investigate the long-term (meta)stability as well as changes in the composition of LiC_{6-x} over time. In addition, more invasive temperature-dependent NMR experiments are performed after 5 months, followed by another 2 months of ageing.

We record static ^{7}Li NMR spectra after 12 days (dark blue curve in Fig. 4) and after 5 months (light blue curve Fig. 4). The sample is thoroughly cleaned before each measurement, exposing golden shiny faces on each side of the HOPG crystal. We observe a decrease in the high-ppm peak intensities, suggesting a partial degradation of the corresponding structures. The degradation process appeared incomplete, with a residual broad signal that appears as the overlap of both shifts (i.e., the sharp

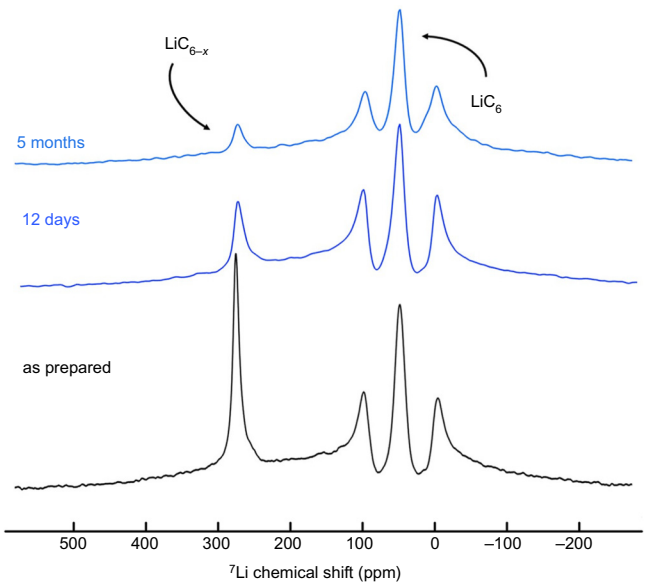

FIG. 4. Evolution of the static ^{7}Li NMR spectrum during ageing of Li-intercalated HOPG. The black curve shows the spectrum recorded after preparation. The dark blue curve shows the spectrum of the same sample aged for 12 days and the light blue curve after ageing for 5 months. The signal appearing at 10–13 ppm overlaps with the quadrupole satellite of LiC_6 and appears more pronounced after 5 months compared to 12 days.

274-ppm feature and the broader 256-ppm shoulder) present in the fresh sample spectrum. The stability of the structures associated with these signals over several months is compatible with Nalimova *et al.* [24]. The 274-ppm signal intensity seems to decrease most during this timeframe but cannot be fully disentangled from the 256 ppm (light blue versus black curve Fig. 4). A new Li environment with a chemical shift of 10–13 ppm forms concomitantly. Signatures in this region are commonly associated with lower SOC and generically identified as LiC_{6+x} [15], or, in other works, attributed to Li—Li dimers [64].

After 5 months the sample decomposed visibly, as shown in Fig. 5. The observed drastic delamination is only compatible with the expulsion of lithium from inside the sample; thus, it would not have occurred if the high-ppm signal was caused by surface metal only. Residual metallic lithium would only be present on the surface of the crystal and thus cannot be the cause of the sudden volume increase at the edges of the sample. Delamination shows more prominently on the side that is cut for the perpendicular control experiment (see Sec. III A). This is due to the fact that the cut created defects at the surface, which are likely to facilitate expulsion of lithium from within, as it is generally known that ion mobility in graphite is enhanced in the presence of defects (as reported, for example, in Ref.

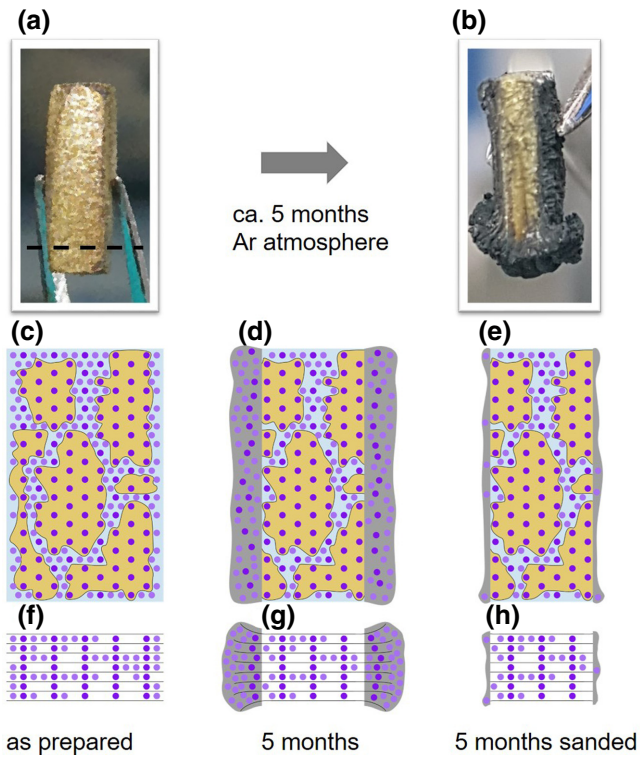

FIG. 5. Representation of the sample. (a) Image of Li intercalated in HOPG after polishing. The golden color indicates LiC_6 or LiC_{6-x} compounds. The dashed black line indicates the cut for orthogonal measurement (cf. Supplementary Fig. S3). (b) The sample after approximately 5 months of calendar ageing in an inert atmosphere. The delamination shows the partial decomposition of the superdense compound and is accentuated along the cut. (c)–(h) Schematic cuts through the overlithiated HOPG sample. Horizontal black lines in (f)–(h) represent graphene layers, and violet dots are Li nuclei. Golden shaded regions represent well-ordered LiC_6 domains, giving rise to the 45-ppm NMR signal (cf. Fig. 3). The blue interdomain region is overlithiated. Note that the dimensions are not drawn to scale. Upon ageing, the surface of the lithiated HOPG crystal delaminates (gray shading), with disordered carbon forming that pulls Li from disordered regions, yet maintaining the LiC_6 domains and the overlithiated interdomain region. Sanding only affects the surface, leaving the inner regions unchanged.

[62]). The opening of the graphite sheets was also previously associated with pressure release from within the bulk material [24,30,33]. This is a further indicator towards the degradation of a superdense structure. Figure 5 also shows a schematic model of possible microscopic configurations of the ageing sample [panels (c) and (f)], with ordered LiC_6 domains and overlithiated interdomain regions. Panels (d) and (g) show the schematic delamination after 5 months. Panels (e) and (h) represent the sample after cleaning.

In the temperature-dependent measurements (Fig. 6 and Supplementary Fig. S4 [22]), the residual high-ppm peak disappears after mild heating to 310–330 K, while the (10–13)-ppm signal becomes more evident

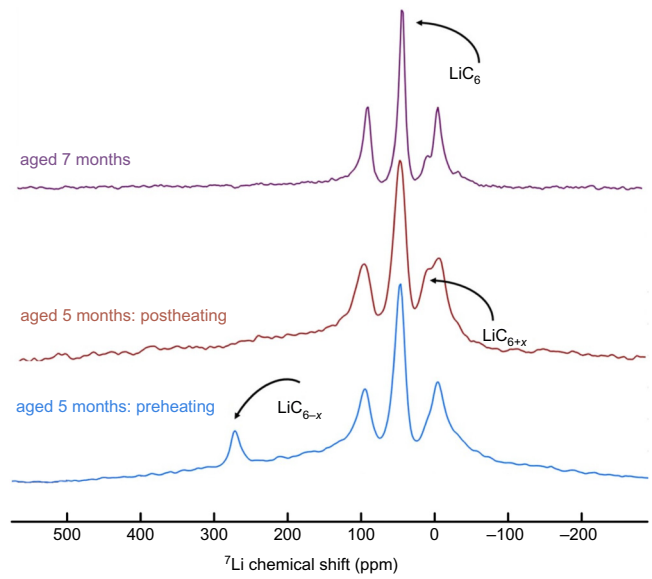

FIG. 6. Static ^{7}Li NMR spectra taken after the decomposition process and pre- and postheating to accelerate the equilibration of the residual superdense phases. All the shown curves correspond to measurements at 25 °C before (blue) and after (red) heating; during the heating process the sample is treated and measured from −10 °C to 60 °C, as shown in Supplementary Fig. S4 [22]. The violet curve shows the sample aged for two additional months. The peak at 10–13 ppm remains stable.

(cf. Supplementary Fig. S4 [22]). The broad spectral feature between about 100–200 ppm, which temporarily vanishes at elevated temperature during the heating cycle (cf. Supplementary Fig. S4 [22] at 40 °C and 60 °C), reappears postheating and only vanishes permanently after two more months of ageing.

C. *Ab initio* thermodynamics and dynamics of superdense GICs

A basic modeling approach is to initially consider periodic high-symmetry structures as shown in Fig. 2, and calculate the formation free energies of these extended "pure" phases. To this end, we adopt an *ab initio* thermodynamics approach [65]. A detailed derivation of the formalism adapted to our system is provided in Sec. II within the Supplemental Material [22]. Within this framework we calculate the free energy of intercalation ΔG^{interc} for the stoichiometries reported in Fig. 2 at 300 and 500 K and ambient pressure. Based on these, we estimate relative populations $N(LiC_{6-x})/N(LiC_6)$ at equilibrium as Boltzmann ratios with respect to LiC_6. The results are reported in Table I. The effect of configurational entropy is neglected, which would further favor overlithiated compounds (except LiC_2; cf. Sec. 2 within the Supplemental Material [22]). As such, the relative populations are to be considered a lower estimate.

With LiC_2 at +1.09 eV (105.17 kJ/mol) at 500 K, we exclude its presence in the sample. However, $LiC_{3.4}$ and $LiC_{4.8}$ have only mildly positive ΔG^{interc} at 500 K, which even becomes negative at room temperature for $LiC_{4.8}$. Correspondingly, their relative populations are nonvanishing.

Further insights can be given by considering, e.g., the insertion of an additional Li atom in a 3×3 LiC_6 supercell. This corresponds to a Li:C ratio of 1.11%. Such a stoichiometry, in its simplest configuration, has only one additional Li atom in any of the empty C_6 hexagonal sites, forming a three-pronged star. The corresponding ΔG of formation is negative in the entire range of considered temperatures, indicating that at least some excess of lithium enters spontaneously, corresponding to already over 10% beyond the theoretical capacity. Already for this stoichiometry, one may construct an alternative configuration which includes a Li_7 cluster—this would correspond to neighboring Li atoms, from the LiC_6 lattice in the immediate surroundings of the excess Li, "aggregating" around the latter. The corresponding ΔG of formation is hereby positive, albeit less than for an extended $LiC_{3.4}$ phase and thus even more thermally accessible.

Based on this simplified energetics, we can conclude that, whereas the formation of an extended $LiC_{3.4}$ phase appears unlikely, the formation of scattered Li_4 and Li_7 islands cannot at all be excluded.

Regardless of the precise assignment of the high-ppm signal (*vide infra*), we stress at this point that the energetics above, albeit simplified, confirms that a certain amount of excess lithium does indeed enter spontaneously. In other words, the common conception that LiC_6 corresponds to 100% SOC is not entirely accurate thermodynamically. The exact upper limit of overlithiation accessible beyond LiC_6 and its dependence on external conditions can only be determined by means of computationally expensive statistical sampling, which goes beyond the scope of this work.

The observed high-ppm signal may indeed arise from Li_7 "flowers" and/or Li_4 "stars" present not only in sizable domains of exact $LiC_{3.4}$ and $LiC_{4.8}$ compositions, but also diluted in a LiC_6 environment. Considering that, starting from a LiC_6 environment, every additional lithium will form at least a Li_4 "star"; this can happen at any LiC_{6-x} stoichiometry. Additionally, a "flower" may form if three neighboring Li atoms from the immediate surroundings aggregate around the center of a "star". We estimate the cost of such aggregation as approximately 0.11 eV, thus also thermally accessible. Subsequently, "star" and "flower" motifs are in equilibrium with each other, and thus both can contribute to the high-ppm signals.

The relative populations at 300 K (cf. Table I) confirm the metastability of superdense patterns at room temperature. However, the relative concentrations of these patterns in the fresh sample must be closer to those at 500 K than those at 300 K, as the calendaric ageing showed a slow equilibration towards degradation.

Assuming that the decomposition is diffusion controlled, we estimate the effective diffusion barrier and thus the relative degradation rate at 300 versus 500 K. We perform *ab initio* molecular dynamics (AIMD) simulations, based on DFTB [53], to evaluate Li mobility in a slightly oversaturated LiC_{6-x} supercell with two Li_7 motifs in a LiC_6-like environment. The resulting diffusion coefficients (Supplementary Fig. S5 [22]) show Arrhenius behavior with an effective barrier of 0.35 eV, which slows down the delithiation about 225 times at room temperature compared to 500 K (see Sec. III within the Supplemental Material [22] for a brief discussion on diffusion coefficients in Li GICs, which includes Refs. [8,17,18,59,66–71]).

We note in passing that the AIMD trajectories exhibited frequent occurrences of directly connected Li dimers and trimers in an isosceles triangular configuration as transient byproducts of the decomposition of the Li_7 clusters (Supplementary Fig. S6 [22]). This nicely ties in with the appearance of the low-ppm shoulder upon ageing, if this were to be attributed to Li—Li dimers rather than low-SOC patterns.

D. Discussion

Without the option (see Sec. VI within the Supplemental Material [22]) to explicitly compute sufficiently converged Knight shifts (see, e.g., Refs. [72–75]), we cannot unambiguously assign each ^{7}Li NMR resonance. We can experimentally exclude the possibility that high-ppm features are generated primarily by lithium metal. On energetic grounds, we also exclude full LiC_2. Thus, we infer the presence of some form of intermediately overlithiated phase containing Li_7 ("flowers") and/or Li_4 ("star") motifs, and associate the high-ppm shift with the pseudometallic character of the central atoms. While one may argue whether the Li_4 stars are "dense" enough to produce high-ppm shifts, their formation is more energetically accessible than that of Li_7 flowers; therefore, a spectroscopic signature is to be expected. In the light of this, we put forward the following scenario, qualitatively combining experimental observations and simulations. The asymmetric high-ppm signal corresponds to sizable domains of at least $LiC_{4.8}$ stoichiometry, possibly mixed with $LiC_{3.4}$, and domains of variable $LiC_{x>3.4}$ stoichiometries with Li_7 and/or Li_4 motifs diluted in LiC_6-like surroundings.

The signal is split into a sharp 274-ppm feature and a broad 256 feature due to susceptibility effects analogously to metallic lithium, but of smaller magnitude. As such, the more intensive 274-ppm peak would correspond to sample faces with normal vectors perpendicular to B_0, while the 256 ppm corresponds to face normals parallel to B_0. It is reasonable to assume that overlithiation mainly occurs in the proximity of the HOPG surface, while the inner bulk

TABLE I. Formation energies of selected LiC_{6-x} intercalation compounds. We calculate ΔE from DFT total energies (cf. Sec. II), not including the zero-point energies nor any finite temperature contribution. The values of ΔG at different temperatures and ambient pressure are calculated using the *ab initio* thermodynamics approach. Our experimental conditions are $T = 500$ K and $P = 1$ atm. Non-negligible populations at 300 and 500 K are indicated in bold.

	LiC_6	$LiC_{4.8}$	$LiC_{3.4}$	LiC_3	$LiC_{2.7}$	LiC_2
ΔE^{interc} (DFT-D3) (eV)	−0.10	−0.01	0.14	0.27	0.46	1.08
ΔG^{interc} (300 K) (eV)	−0.12	−0.03	0.09	0.24	0.40	1.00
ΔG^{interc} (500 K) (eV)	−0.09	0.02	0.12	0.28	0.44	1.09
$N(LiC_{6-x})/N(LiC_6)$ (300 K)	···	**0.03**	0.00	0.00	0.00	0.00
$N(LiC_{6-x})/N(LiC_6)$ (500 K)	···	**0.08**	**0.01**	0.00	0.00	0.00

is predominantly LiC_6. Then, the relative magnitude of the two peaks reflects the dimensions of the sample (longer surface along B_0). Moreover, as the core of the sample may be shielded to a fair degree, surface species may be weighted more strongly and therefore show a higher relative amplitude with respect to the LiC_6 bulk than relative energetics would suggest [76].

Considering the inherent metastability of Li_7 clusters, an additional significant population of imperfect Li_n clusters (with $3 \leq n < 7$) can be expected ("broken flowers"). The lithium atoms belonging to these clusters are undercoordinated with respect to the Li_7 central atom but still occupying adjacent C_6 rings. Therefore, they can be expected to produce a signal at a higher shift than the lithium atoms in LiC_6. Li_3 motifs can analogously appear as "broken stars." Additionally, both the crown atoms of the Li_7 and the prongs of the Li_4 motifs have lower coordination than the respective central atoms. As such, there are many possible realizations of microstructures with a wide range of coordinations. Thus, we may attribute the broad spectral feature at 100–200 ppm to a superposition of resonances corresponding to all of the above species.

The decrease of both the high-ppm peaks and the broad (100–200)-ppm spectral feature are correlated with the increase of the (10–13)-ppm feature. This is a strong indication that the degradation of superdense structures directly corresponds to the appearance of a new Li environment. In line with previous assignments of the low-ppm feature in the literature [15], this can correspond to either Li—Li dimers occurring as the smallest possible decomposition product before LiC_6-like Li, or to the formation of locally Li-depleted LiC_{6+x} regions following the ejection of Li at the surface. Of note, these two patterns can coexist as a result of decomposition (cf. Supplementary Fig. S6 [22]) or, in an electrochemical context, due to deintercalation.

Without attempting a quantitative estimation of the excess capacity, we can roughly place it in the order of 1% to 10% based on the relative populations in Table I and a qualitative inspection of the relative magnitude of the observed peaks. Clearly, this is not a huge number; as such, we are not claiming that graphitic battery anodes should be pushed beyond the currently accepted limit of 100% SOC in commercial applications, only to obtain a negligible gain in capacity. The primary implications of these findings do not lie in the practically achievable capacity limit. Instead, performance-critical phenomena, such as lithium plating and dendrite formation, often occur at the upper limit of intercalation, and details of the involved mechanisms are still unclear.

For a mechanistic understanding and knowledge-based engineering, a comprehensive picture of structural motifs and processes occurring at the atomistic level when approaching this limit is essential. In our view, the common assumption that LiC_6 represents a well-defined upper limit for Li intercalation poses the danger of misinterpreting the conditions at which these phenomena occur and, thereby, mistake correlation for causality. In addition, experimental evidence may at least be partially misinterpreted, or potential explanations could easily be overlooked [77,78].

It is reasonable to expect that overlithiation occurs just as well under electrochemical conditions. The applied potential provides an additional driving force towards (over)intercalation, which becomes substantially stronger than high temperature—the sole driving force in the presented results—at increasing C rates. For example, although not for HOPG but for microcrystalline graphite, Sole *et al.* [79] did observe the consumption of a larger amount of lithium during the first charge cycle, which "disappeared" after the first cycle. They attributed the phenomenon to solid electrolyte interface formation. In the light of our findings, the possibility of overintercalation and its potential impact should also be considered as a possible influencing factor.

In particular, we speculate that the drastic mobility drop may play a significant role in the onset of lithium plating and dendrite formation, due to the transport bottleneck emerging at the interface and subsequently triggering an overshoot in the Li chemical potential [80,81]. The detailed understanding of this mechanism cannot neglect the occurrence of overlithiation, as variations in ion mobility are expected to occur before, at, and beyond LiC_6.

The exact quantitative variation of mobility versus SOC at the upper limit has yet to be investigated, e.g., by means of kinetic Monte Carlo simulations, specifically targeted to battery materials with a correct description of the electrostatic interaction between charge carriers [82–85], and one- and two-dimensional continuum models for mass and charge transport [86], and is expected to be nontrivial given the highly ordered nature of LiC_6 and the disordered nature of any composition shortly below and beyond. To complicate things further, from the modeling point of view, slow or frustrated dynamics favors the occurrence of nonequilibrium phenomena, which are scarcely modeled in the field. All the above considerations are particularly important under fast-charging conditions, where nonequilibrium effects become predominant [87].

Moreover, there is a fundamental difference in the chemical nature of lithium ion local environments between LiC_6-like (or lower) and "superdense" patterns—the latter being essentially metallic nanoclusters with shorter Li-Li distances. As such, negating their presence at the interface at the upper limit of intercalation simply means neglecting possible nucleation precursors [88]. As an additional consideration, our calculations show that the energy penalty associated with two lithium atoms occupying nearest-neighbor positions is not insurmountably large, meaning that these moieties may already occur locally before reaching bulk LiC_6 stoichiometry, especially considering the slow nonequilibrium insertion dynamics. Under electrochemical drive, the charging process is faster than the slow infiltration we observe. Thus, overlithiation is likely to remain confined at the charging interface, due to the aforementioned mobility drop, and even occur at the interface before full lithiation is achieved globally. There is evidence of inhomogeneity in charging processes, leading to gradients in Li concentration across anode particles. This phenomenon is largely accentuated under fast-charging conditions, as reported, for example, in Ref. [77], where the effect of increasing the C rate causing inhomogeneous lithium concentrations is apparent. While it is difficult to disentangle the effect of diffusion in the electrolyte around the graphite grains from the diffusion into the grains in a complex sample under electrochemical conditions, it is still clear that the Li chemical potential in the golden region must be higher in the fast-charging case due to the limited macroscopic mass transport.

Finally, the consideration of local superdense motifs can shed additional light on carbonaceous materials for which the possibility to reach higher capacity is already known. So-called high specific charge carbons are known to incorporate higher than 1:6 ratios of lithium under electrochemical conditions (see, e.g., Ref. [62]). Although these are nongraphitic forms of carbon, several of the models proposed refer to graphitic or graphene structural C motifs (e.g., Sato *et al.* [64], who also included NMR data). In the light of our findings, an additional angle when looking at these high specific charge carbons could be provided by considering the access of Li to the graphitic layers, rather than only in amorphous or defect-rich regions, i.e., that carbon could, and would, accommodate additional Li, but that the potential for insertion becomes lower than for metallic Li after a certain loading threshold.

However, we can only acknowledge all these implications once we accept the notion of spontaneous overintercalation, which itself defies the assumption that lithium ions can only occupy nearest-neighbor positions under high pressure, or as a metastable result of decomposition of high-pressure superdense compounds. This assumption was previously identified as the reason for the instability of the latter, and it is not supported by energetics.

Given that the reported results were beyond the initial objectives of our study (to recall, producing well-defined reference data to facilitate the interpretation of more complex *in operando* experiments), a quantitative characterization was not attempted and cannot be performed as postprocessing analysis of our data due to the loss of an unknown amount of mass after mechanical polishing at every measurement. In the perspective of reproducibility, such a quantitative interpretation necessitates the consideration of ordered and disordered structural features in combination with dynamic processes that cover time constants from picoseconds (see Sec. III within the Supplemental Material [22]) to months (duration over which the presented experiments were conducted). In addition, quantitativity would have to be established first for this type of sample for most of the commonly employed analytical techniques. Also, there are not many techniques that would be able to unambiguously distinguish between a LiC_6-LiC_{6+x} sample and a LiC_6-LiC_{6-x} sample—which we, in passing, identify as one of the main reasons why spontaneous overintercalation remained overlooked for such a long time.

X-ray diffraction is problematic due to the close similarity of the c parameter of all stage-I compounds. Our calculations do not find a significant variation of the interlayer distance, except an observed contraction for LiC_2, which is not energetically plausible anyway. Previous works [24,25,30] report the same interlayer distance even up to LiC_2, with the caveat that the exact composition of the sample was unknown after releasing the pressure. To complicate things further, even if, for example, theoretical calculations would have shown a significant change in interlayer distance, that would have been referred to a pure, extended phase corresponding to standard periodic boundary condition DFT calculations, and would likely not apply to overlithiated islands in an otherwise LiC_6-like matrix.

Neutron diffraction, on the other hand, detects lithium directly and has been employed to investigate lithium plating [89], and thus would be suitable in principle, but the expected variations in the spectra are below the detection limit. We made preliminary calculations of

diffraction patterns for neutron radiation diffraction (as well as x-ray diffraction) in order to test the feasibility of tackling proper phase identification unambiguously with these well-established methods. The simulation results are available online [90]. However, these calculations (see Sec. IV within the Supplemental Material [22]) made clear that it is nearly impossible to obtain the desired unambiguity with this method. The calculations even reveal that one should critically rethink diffraction results published so far, especially if they are based on the interpretation of just a few or even just the single strongest peak (the 0 0 l reflections). A more detailed analysis of the diffraction ambiguity of GICs will be published elsewhere.

Raman spectroscopy is to some extent a promising means to identify signatures of overintercalation. Previous work identifies a peak at 1850 cm^{-1} as a signature of high lithium content [91]; however, that peak is confidently assigned to the stretching of the triple C—C bond in lithium acetylide Li_2C_2. We have no indication of the presence of the latter in our sample, as we do not see any characteristic NMR signature as reported in, e.g., Ref. [92]. Interestingly, this work also reports a resonance at 261 ppm, which is usually attributed to residual lithium metal. However, the formation of acetylidelike intermediates may occur at the graphite surface during the intercalation process as part of the insertion mechanism. Most likely, these become quantitatively detectable only once the uptake slows down critically when approaching (and then exceeding) LiC_6, which explains the appearance of the signal just before plating and its disappearance after. On the other hand, there is no previous literature reporting Raman spectra of intermediate compositions between LiC_6 and LiC_2. However, a simple inspection of the phonon densities of states (see Sec. V within the Supplemental Material [22]) suggests that the most prominent variations due to overintercalation manifest at frequencies lower than 500 cm^{-1}, which can be difficult to detect (although recent *in operando* Raman spectroscopy work on lithium intercalation in graphite shows that the detection of low-frequency features is not out of grasp [93]), while above 500 cm^{-1} the differences in phonon densities of state are small enough to expect Raman experiments directly targeted at LiC_{6-x} to be fairly inconclusive.

Complementary to spectroscopy, gravimetric analysis may also be considered. With the preparation technique used herein, an obvious, immediate complication is the necessity to polish the sample after intercalation in order to ensure that no metallic lithium is present. This hinders a simple weighing experiment before and after intercalation due to loss of mass of unknown amount and composition. Therefore, any attempt at gravimetric analysis has to be performed taking the intercalated, polished sample as a reference and operating in discharge—regardless of the chosen gravimetric technique. While this is in principle possible, we have to remark that complete discharge is not an easy task, and quantifying the residual intercalated lithium, whose amount may be comparable to that of overintercalated lithium, creates a chicken-and-egg problem [41].

In summary, solid-state NMR is likely the most suitable investigation technique due to its high sensitivity to *local* environment and noninvasivity. In further experiments, it may be considered to also record spectra during the infiltration period. We would not expect the peak to appear immediately, but only towards the end. Alternatively, similar patterns may be searched for using electrochemical intercalation. However, in the latter case, even for NMR it is experimentally difficult to clearly disambiguate different overlithiated phases in the LiC_2 to LiC_6 region due to the potential signal overlap of Li metal with the resonances of different LiC_x ($2 \leq x < 6$) species. Chemical shift simulations [94] may be able to help with such an assignment, but will require establishing the necessary methodology for this type of sample first.

Nonetheless, other experimental techniques may also provide signatures for local Li intercalation in graphite beyond LiC_6, and systematic investigations for their identification appear worthwhile.

IV. CONCLUSIONS

While preparing a reference sample of fully lithium-intercalated HOPG for ^{7}Li NMR spectroscopy, we observed unexpected high-ppm resonances. Confidently ruling out that these signatures arise from residual metallic lithium, we attribute them to superdense LiC_{6-x} contributions formed under ambient pressure. We investigate the evolution of the signal under calendaric ageing and rationalize the observations with *ab initio* simulations. We infer that the signal arises from sizable domains containing Li_7 ("flowers") and/or Li_4 ("stars") motifs in sufficient amounts, and we estimate their long-term (meta)stability. *Ab initio* thermodynamics confirms that a non-negligible excess of lithium enters spontaneously, which, to the best of our knowledge, had never been considered before in graphitic carbon. These findings challenge the currently accepted hypothesis that, since LiC_2 can only be prepared under high pressure [24,30,34], any additional intercalation beyond LiC_6 is implausible.

In hindsight, the simple consideration that the range of stoichiometries between LiC_6 and LiC_2 spans 200% states of charge beyond the commonly accepted 100% SOC Li loading of graphite should suggest prudence in such an assumption. Yet, it was never rigorously verified. In our view, multiple previous works on electrochemical cells contain indications compatible with at least a sparkle of doubt [35,36,38]. In addition, the question of assessing the true capacity of ordered graphitic hosts was explicitly addressed for bilayer or multilayer graphene [95,96]. However, the evidence of overlithiation in the latter did not

reopen the question of analogous occurrence in extended graphite—which is the material actually used in working batteries. For decades, superdense graphite intercalation compounds have been considered only accessible as decomposition products of LiC_2 under high-pressure synthesis ("from above") [24,30,34]. Here we confirm that superdense compositions are also accessible directly as overintercalation products of LiC_6 at ambient pressure ("from below"). If this is possible under the synthesis conditions employed here, it is reasonable to expect that overlithiation is further favored under an applied potential. Particularly in fast-charging conditions, lithium plating is also increasingly favored [77]. Hence, the most intriguing aspect is the interplay of partially reversible plating, overlithiation, and reintercalation. On this account, a reconsideration of the role of overlithiation, so far excluded from the picture with graphite as a host, is warranted. We suggest that the drastic mobility drop associated with the upper limit of intercalation could cause ion clogging at the interface, thus contributing to the onset of lithium plating [80,81]. Under fast-charging conditions, in particular, the inhomogeneity of the intercalation process may play an additional role, as oversaturated regions likely appear already before 100% state of charge is formally reached [77]. Taking overlithiation into consideration may also shed light on other hitherto unexplained phenomena, such as the apparent "disappearance" of some amount of available lithium between cycles, the latter commonly attributed solely to the formation of solid electrolyte interfaces and "dead" lithium [79]. Finally, with regards to the use of NMR for the detection of plating and dendrite formation, our results also suggest that caution is indicated with assigning high-ppm signals nonspecifically to the emergence of metallic lithium deposits.

ACKNOWLEDGMENTS

All the authors thank P. Philipp M. Schleker and Svitlana Taranenko for valuable contributions to experimental aspects of this project and for valuable discussions on NMR, and Matthias Kick and Simon Anniés for fruitful discussions on the theory and data presentation. This work is funded by the German Federal Ministry of Education and Research (BMBF) as part of the research cluster "AQua" within the project InOPlaBat (Grant No. 03XP0352), by the research initiative Jülich Aachen Research Alliance (JARA), section JARA-Energy, within the project MF 001-17 (Project ID G:(DE-82)ZUK2-SF-JARA-ENERGY MF 001-17), and by the German Research Foundation (DFG) as part of the collaborative research center CRC 1114 "Scaling Cascades in Complex Systems" (Project No. 235221301). The authors gratefully acknowledge the computational and data resources provided by the Leibniz Supercomputing Centre (LRZ).

[1] Paris agreement, https://unfccc.int/sites/default/files/english_paris_agreement.pdf (2015), United Nations Treaty.
[2] A. Eftekhari, Lithium-ion batteries with high rate capabilities, ACS Sustain. Chem. Eng. **5**, 2799 (2017).
[3] J.-M. Tarascon and M. Armand, Issues and challenges facing rechargeable lithium batteries., Nature **414**, 359 (2001).
[4] M. Armand and J.-M. Tarascon, Building better batteries, Nature **451**, 652 (2008).
[5] Y. Liu, Y. Zhu, and Y. Cui, Challenges and opportunities towards fast-charging battery materials, Nat. Energy **4**, 540 (2019).
[6] W. Cai, Y.-X. Yao, G.-L. Zhu, C. Yan, L.-L. Jiang, C. He, J.-Q. Huang, and Q. Zhang, A review on energy chemistry of fast-charging anodes, Chem. Soc. Rev. **49**, 3806 (2020).
[7] M. N. Obrovac and V. L. Chevrier, Alloy negative electrodes for Li-ion batteries, Chem. Rev. **114**, 11444 (2014).
[8] J. Asenbauer, T. Eisenmann, M. Kuenzel, A. Kazzazi, Z. Chen, and D. Bresser, The success story of graphite as a lithium-ion anode material – fundamentals, remaining challenges, and recent developments including silicon (oxide) composites, Sustain. Energy Fuels **4**, 5387 (2020).
[9] M. S. Dresselhaus and G. Dresselhaus, Intercalation compounds of graphite, Adv. Phys. **51**, 1 (2002).
[10] J. R. Dahn, T. Zheng, Y. Liu, and J. S. Xue, Mechanisms for lithium insertion in carbonaceous materials, Science **270**, 590 (1995).
[11] J. Conard, V. A. Nalimova, and D. Guérard, NMR study of LiC_x graphite intercalation compounds prepared under high pressure, Mol. Cryst. Liq. Cryst. Sci. Technol. Sect. A. Mol. Cryst. Liq. Cryst. **245**, 25 (1994).
[12] S. Rabii and D. Guérard, Stability of superdense lithium graphite compounds, J. Phys. Chem. Solids **69**, 1165 (2008).
[13] O. Pecher, J. Carretero-González, K. J. Griffith, and C. P. Grey, Materials' methods: NMR in battery research, Chem. Mater. **29**, 213 (2016).
[14] S. A. Kayser, A. Mester, A. Mertens, P. Jakes, R.-A. Eichel, and J. Granwehr, Long-run in operando NMR to investigate the evolution and degradation of battery cells, Phys. Chem. Chem. Phys. **20**, 13765 (2018).
[15] J. L. L. Lopez, P. J. Grandinetti, and A. C. Co, Enhancing the real-time detection of phase changes in lithium–graphite intercalated compounds through derivative operando (dOp) NMR cyclic voltammetry, J. Mater. Chem. A **6**, 231 (2018).
[16] R. L. Sacci, L. W. Gill, E. W. Hagaman, and N. J. Dudney, Operando NMR and XRD study of chemically synthesized LiC oxidation in a dry room environment, J. Power Sources **287**, 253 (2015).
[17] K. Persson, V. A. Sethuraman, L. J. Hardwick, Y. Hinuma, Y. S. Meng, A. van der Ven, V. Srinivasan, R. Kostecki, and G. Ceder, Lithium diffusion in graphitic carbon, J. Phys. Chem. Lett. **1**, 1176 (2010).
[18] I. Umegaki, S. Kawauchi, H. Sawada, H. Nozaki, Y. Higuchi, K. Miwa, Y. Kondo, M. Månsson, M. Telling, F. C. Coomer, S. P. Cottrell, T. Sasaki, T. Kobayashi, and J. Sugiyama, Li-ion diffusion in Li intercalated graphite C_6Li and $C_{12}Li$ probed by μ^+SR, Phys. Chem. Chem. Phys. **19**, 19058 (2017).
[19] J. Conard and H. Estrade, Résonance magnétique nucléaire du lithium interstitiel dans le graphite, Mater. Sci. Eng. **31**, 173 (1977).

[20] D. Guérard and A. Hérold, Intercalation of lithium into graphite and other carbons, Carbon **13**, 337 (1975).
[21] J. Duan, Y. Zheng, W. Luo, W. Wu, T. Wang, Y. Xie, S. Li, J. Li, and Y. Huang, Is graphite lithiophobic or lithiophilic?, Natl. Sci. Rev. **7**, 1208 (2020).
[22] See Supplemental Material at http://link.aps.org/supplemental/10.1103/PRXEnergy.2.013003 for additional details on the sample preparation, on the computational approach, on the temperature-dependent experiments, and for additional discussion of alternative experimental and computational characterizations.
[23] W. Schülke, A. Berthold, and A. Kaprolat, Information about the band structure of LiC_6 from inelastic synchrotron x-ray scattering, Synth. Met. **34**, 423 (1989).
[24] V. Nalimova, D. Guérard, M. Lelaurain, and O. Fateev, X-ray investigation of highly saturated Li-graphite intercalation compound, Carbon **33**, 177 (1995).
[25] C. Bindra, V. A. Nalimova, D. E. Sklovsky, W. A. Kamitakahara, and J. E. Fischer, Statics and dynamics of interlayer interactions in the dense high-pressure graphite compound LiC_2, Phys. Rev. B **57**, 5182 (1998).
[26] G. Bondarenko, V. A. Nalimova, O. Fateev, D. Guérard, and K. N. Semenenko, Vibrational spectra of superdense lithium graphite intercalation compounds, Carbon **36**, 1107 (1998).
[27] A. Schirmer, P. Heitjans, and V. A. Nalimova, Conduction-electron induced spin-lattice relaxation of ^{8}Li in the high-pressure phase LiC_2, Mol. Cryst. Liq. Cryst. Sci. Technol. Sect. A. Mol. Cryst. Liq. Cryst. **310**, 291 (1998).
[28] D. Guérard and R. Janot, Structure of the superdense LiC_3 compound prepared by ball-milling, J. Phys. Chem. Solids **65**, 147 (2004).
[29] R. Setton and J. Conard, Madelung energy and stability of the compound Li_7C_{24} prepared under pressure, Mol. Cryst. Liq. Cryst. Sci. Technol. Sect. A. Mol. Cryst. Liq. Cryst. **244**, 307 (1994).
[30] V. Z. Mordkovich, Synthesis and XPS investigation of superdense lithium-graphite intercalation compound, LiC_2, Synth. Met. **80**, 243 (1996).
[31] R. Janot and D. Guérard, Ball-milling in liquid media: Applications to the preparation of anodic materials for lithium-ion batteries, Prog. Mater. Sci. **50**, 1 (2005).
[32] C. Burmeister, L. Titscher, S. Breitung-Faes, and A. Kwade, Dry grinding in planetary ball mills: Evaluation of a stressing model, Adv. Powder Technol. **29**, 191 (2018).
[33] V. A. Nalimova, High pressure for synthesis and study of superdense alkali metal - carbon compounds, Mol. Cryst. Liq. Cryst. Sci. Technol. Sect. A. Mol. Cryst. Liq. Cryst. **310**, 5 (1998).
[34] J. Conard and P. Lauginie, Lithium NMR in lithium-carbon solid state compounds, TANSO **2000**, 62 (2000).
[35] S. E. Hayes, R. A. Guidotti, W. R. Even, P. J. Hughes, and H. Eckert, ^{7}Li solid-state nuclear magnetic resonance as a probe of lithium species in microporous carbon anodes, J. Phys. Chem. A **107**, 3866 (2003).
[36] R. Tossici, R. Janot, F. Nobili, D. Guérard, and R. Marassi, Electrochemical behavior of superdense 'LiC_2' prepared by ball-milling, Electrochim. Acta **48**, 1419 (2003).
[37] P. Azaïs, L. Duclaux, A.-M. Faugère, and F. Béguin, Reactive milling of graphite with lithium: Application to lithium batteries, Appl. Phys. Lett. **81**, 775 (2002).
[38] T. M. Paronyan, A. K. Thapa, A. Sherehiy, J. B. Jasinski, and J. S. D. Jangam, Incommensurate graphene foam as a high capacity lithium intercalation anode, Sci. Rep. **7**, 2045 (2017).
[39] V. V. Avdeev, V. A. Nalimova, and K. N. Semenenko, The alkali metals in graphite matrixes-new aspects of metallic state chemistry, High Press. Res. **6**, 11 (1990).
[40] Y. F. Reynier, R. Yazami, and B. Fultz, Thermodynamics of lithium intercalation into graphites and disordered carbons, J. Electrochem. Soc. **151**, A422 (2004).
[41] Y. Reynier, R. Yazami, and B. Fultz, XRD evidence of macroscopic composition inhomogeneities in the graphite–lithium electrode, J. Power Sources **165**, 616 (2007).
[42] M. Drüe, M. Seyring, A. Kozlov, X. Song, R. Schmid-Fetzer, and M. Rettenmayr, Thermodynamic stability of Li_2C_2 and LiC_6, J. Alloys Compd. **575**, 403 (2013).
[43] Y. Imai and A. Watanabe, Energetic evaluation of possible stacking structures of Li-intercalation in graphite using a first-principle pseudopotential calculation, J. Alloys Compd. **439**, 258 (2007).
[44] Z. Wang, S. M. Selbach, and T. Grande, Van der Waals density functional study of the energetics of alkali metal intercalation in graphite, RSC Adv. **4**, 3973 (2014).
[45] C.-H. Doh, B.-C. Han, B.-S. Jin, and H.-B. Gu, Structures and formation energies of Li_xC_6 ($x = 1 - 3$) and its homologues for lithium rechargeable batteries, Bull. Korean Chem. Soc. **32**, 2045 (2011).
[46] G. Roth, K. Lüders, P. Pfluger, and H.-J. Güntherodt, ^{7}Li and ^{133}Cs NMR parameters in C_6Li and C_8Cs intercalated oriented graphites, Solid State Commun. **39**, 423 (1981).
[47] G. Kresse and J. Hafner, Ab initio molecular dynamics for liquid metals, Phys. Rev. B **47**, 558 (1993).
[48] J. P. Perdew, K. Burke, and M. Ernzerhof, Generalized Gradient Approximation Made Simple, Phys. Rev. Lett. **77**, 3865 (1996).
[49] G. Kresse and D. Joubert, From ultrasoft pseudopotentials to the projector augmented-wave method, Phys. Rev. B **59**, 1758 (1999).
[50] S. Grimme, J. Antony, S. Ehrlich, and H. Krieg, A consistent and accurate ab initio parametrization of density functional dispersion correction (DFT-D) for the 94 elements H-Pu, J. Chem. Phys. **132**, 154104 (2010).
[51] A. Togo and I. Tanaka, First principles phonon calculations in materials science, Scr. Mater. **108**, 1 (2015).
[52] M. Chase, *NIST-JANAF thermochemical tables* (American Institute of Physics, College Park, MD, 1998), 4th ed.
[53] M. Elstner, D. Porezag, G. Jungnickel, J. Elsner, M. Haugk, T. Frauenheim, S. Suhai, and G. Seifert, Self-consistent-charge density-functional tight-binding method for simulations of complex materials properties, Phys. Rev. B **58**, 7260 (1998).
[54] B. Hourahine, *et al.*, DFTB+, a software package for efficient approximate density functional theory based atomistic simulations, J. Chem. Phys. **152**, 124101 (2020).
[55] C. Panosetti, S. Anniés, C. Grosu, S. Seidlmayer, and C. Scheurer, DFTB modeling of lithium-intercalated graphite with machine-learned repulsive potential, J. Phys. Chem. A **125**, 691 (2021).
[56] S. Anniés, C. Panosetti, M. Voronenko, D. Mauth, C. Rahe, and C. Scheurer, Accessing structural, electronic, transport

and mesoscale properties of Li-GICs via a complete DFTB model with machine-learned repulsion potential, Materials **14**, 6633 (2021).

[57] D. J. Evans and B. L. Holian, The Nose–Hoover thermostat, J. Chem. Phys. **83**, 4069 (1985).

[58] P. Lauginie, H. Estrade-Szwarckopf, and J. Conard, ^{6}Li, ^{7}Li and ^{8}Li-NMR shifts and relaxation rates in LiC_6: Evidence of quadrupolar interaction with conduction electrons, Mater. Sci. Forum **91-93**, 545 (1992).

[59] J. Langer, V. Epp, P. Heitjans, F. A. Mautner, and M. Wilkening, Lithium motion in the anode material LiC_6 as seen via time-domain ^{7}Li NMR, Phys. Rev. B **88**, 094304 (2013).

[60] R. Bhattacharyya, B. Key, H. Chen, A. S. Best, A. F. Hollenkamp, and C. P. Grey, In situ NMR observation of the formation of metallic lithium microstructures in lithium batteries, Nat. Mater. **9**, 504 (2010).

[61] H. J. Chang, A. J. Ilott, N. M. Trease, M. Mohammadi, A. Jerschow, and C. P. Grey, Correlating microstructural lithium metal growth with electrolyte salt depletion in lithium batteries using ^{7}Li MRI, J. Am. Chem. Soc. **137**, 15209 (2015).

[62] M. Winter, J. O. Besenhard, M. E. Spahr, and P. Novák, Insertion electrode materials for rechargeable lithium batteries, Adv. Mater. **10**, 725 (1998).

[63] N. M. Trease, L. Zhou, H. J. Chang, B. Y. Zhu, and C. P. Grey, In situ NMR of lithium ion batteries: Bulk susceptibility effects and practical considerations, Solid State Nucl. Magn. Reson. **42**, 62 (2012).

[64] K. Sato, M. Noguchi, A. Demachi, N. Oki, and M. Endo, A mechanism of lithium storage in disordered carbons, Science **264**, 556 (1994).

[65] J. Rogal and K. Reuter, in *Experiment, Modeling and Simulation of Gas Surface Interactions for Reactive Flows in Hypersonic Flights* (2007).

[66] A. Magerl, H. Zabel, and I. S. Anderson, In-Plane Jump Diffusion of Li in LiC_6, Phys. Rev. Lett. **55**, 222 (1985).

[67] Y. NuLi, J. Yang, and Z. Jiang, Intercalation of lithium ions into bulk and powder highly oriented pyrolytic graphite, J. Phys. Chem. Solids **67**, 882 (2006).

[68] K. Toyoura, Y. Koyama, A. Kuwabara, F. Oba, and I. Tanaka, First-principles approach to chemical diffusion of lithium atoms in a graphite intercalation compound, Phys. Rev. B **78**, 135502 (2008).

[69] K. Toyoura, Y. Koyama, A. Kuwabara, and I. Tanaka, Effects of off-stoichiometry of LiC_6 on the lithium diffusion mechanism and diffusivity by first principles calculations, J. Phys. Chem. C **114**, 2375 (2010).

[70] K. Dokko, N. Nakata, Y. Suzuki, and K. Kanamura, High-rate lithium deintercalation from lithiated graphite single-particle electrode, J. Phys. Chem. C **114**, 8646 (2010).

[71] N. Takami, A. Satoh, M. Hara, and T. Ohsaki, Structural and kinetic characterization of lithium intercalation into carbon anodes for secondary lithium batteries, J. Electrochem. Soc. **142**, 371 (2019).

[72] R. Laskowski and P. Blaha, NMR shielding in metals using the augmented plane wave method, J. Phys. Chem. C **119**, 19390 (2015).

[73] A. R. Ferreira, K. Reuter, and C. Scheurer, Toward routine gauge-including projector augmented-wave calculations for metallic systems: The case of ScT_2Al (T = Ni, Pd, Pt, Cu, Ag, Au) Heusler phases, J. Phys. Chem. C **120**, 25530 (2016).

[74] A. R. Ferreira, DFT-GIPAW ^{27}Al NMR simulations for intermetallics: Accuracy issues and magnetic screening mechanisms, J. Phys. Chem. C **123**, 9371 (2019).

[75] C. Tantardini, A. G. Kvashnin, and D. Ceresoli, GIPAW pseudopotentials of d elements for solid-state NMR, Materials **15**, 3347 (2022).

[76] J. Winter, *Magnetic resonance in metals* (Clarendon Press Oxford, 1971) pp. xiii, 206 p.

[77] J. Wandt, P. Jakes, J. Granwehr, R.-A. Eichel, and H. A. Gasteiger, Quantitative and time-resolved detection of lithium plating on graphite anodes in lithium ion batteries, Mater. Today **21**, 231 (2018).

[78] S. Jovanovic, P. Jakes, S. Merz, R.-A. Eichel, and J. Granwehr, Lithium intercalation into graphite: In operando analysis of Raman signal widths, Electrochem. Sci. Adv. **2**, 2698 (2021).

[79] C. Sole, N. E. Drewett, and L. J. Hardwick, Insitu Raman study of lithium-ion intercalation into microcrystalline graphite, Faraday Discuss. **172**, 223 (2014).

[80] H.-K. Tian, Z. Liu, Y. Ji, L.-Q. Chen, and Y. Qi, Interfacial electronic properties dictate Li dendrite growth in solid electrolytes, Chem. Mater. **31**, 7351 (2019).

[81] Y. Dong, Z. Zhang, A. Alvarez, and I.-W. Chen, Potential jumps at transport bottlenecks cause instability of nominally ionic solid electrolytes in electrochemical cells, Acta Mater. **199**, 264 (2020).

[82] E. M. Gavilán-Arriazu, O. A. Pinto, B. L. De Mishima, D. Barraco, O. A. Oviedo, and E. P. M. Leiva, Kinetic Monte Carlo applied to the electrochemical study of the Li-ion graphite system, Electrochim. Acta **331**, 135439 (2020).

[83] E. M. Gavilán-Arriazu, M. Mercer, D. E. Barraco, H. Hoster, and E. Leiva, Kinetic Monte Carlo simulations applied to Li-ion and post Li-ion batteries: A key link in the multi-scale chain, Progress in Energy (2021).

[84] R. N. Methekar, P. W. Northrop, K. Chen, R. D. Braatz, and V. R. Subramanian, Kinetic Monte Carlo simulation of surface heterogeneity in graphite anodes for lithium-ion batteries: Passive layer formation, J. Electrochem. Soc. **158**, A363 (2011).

[85] J. M. Dean, S. W. Coles, W. R. Saunders, A. R. McCluskey, M. J. Wolf, A. B. Walker, and B. J. Morgan, Overscreening and Underscreening in Solid-Electrolyte Grain Boundary Space-Charge Layers, Phys. Rev. Lett. **127**, 135502 (2021).

[86] S. Hein, T. Danner, and A. Latz, An electrochemical model of lithium plating and stripping in lithium ion batteries, ACS Appl. Energy Mater. **3**, 8519 (2020).

[87] R. Tian, S.-H. Park, P. J. King, G. Cunningham, J. Coelho, V. Nicolosi, and J. N. Coleman, Quantifying the factors limiting rate performance in battery electrodes, Nat. Commun. **10**, 1933 (2019).

[88] A. Bhandari, C. Peng, J. Dziedzic, J. R. Owen, D. Kramer, and C.-K. Skylaris, Li nucleation on the graphite anode under potential control in Li-ion batteries, J. Mater. Chem. A **10**, 11426 (2022).

[89] V. Zinth, C. von Lüders, M. Hofmann, J. Hattendorff, I. Buchberger, S. Erhard, J. Rebelo-Kornmeier, A. Jossen, and R. Gilles, Lithium plating in lithium-ion batteries at sub-ambient temperatures investigated by in situ neutron diffraction, J. Power Sources **271**, 152 (2014).

[90] S. Seidlmayer, and C. Panosetti, ND and XRD simulation data of selected Li-GICs (data repository), https://doi.org/10.17617/3.5Z15UH (2022).

[91] M. Cabañero, M. Hagen, and E. Quiroga-González, In-operando Raman study of lithium plating on graphite electrodes of lithium ion batteries, Electrochim. Acta **374**, 137487 (2021).

[92] B. Ruprecht, H. Billetter, U. Ruschewitz, and M. Wilkening, Ultra-slow Li ion dynamics in Li_2C_2—on the similarities of results from ^{7}Li spin-alignment echo NMR and impedance spectroscopy, J. Phys.: Condens. Matter **22**, 245901 (2010).

[93] H. Yadegari, M. A. Koronfel, K. Wang, D. B. Thornton, I. E. L. Stephens, C. Molteni, P. D. Haynes, and M. P. Ryan, Operando measurement of layer breathing modes in lithiated graphite, ACS Energy Lett., 1633 (2021).

[94] S. Köcher, P. Schleker, M. Graf, R.-A. Eichel, K. Reuter, J. Granwehr, and C. Scheurer, Chemical shift reference scale for Li solid state NMR derived by first-principles DFT calculations, J. Magn. Reson. **297**, 33 (2018).

[95] M. Kühne, F. Börrnert, S. Fecher, M. Ghorbani-Asl, J. Biskupek, D. Samuelis, A. V. Krasheninnikov, U. Kaiser, and J. H. Smet, Reversible superdense ordering of lithium between two graphene sheets, Nature **564**, 234 (2018).

[96] K. Ji, J. Han, A. Hirata, T. Fujita, Y. Shen, S. Ning, P. Liu, H. Kashani, Y. Tian, Y. Ito, J. Fujita, and Y. Oyama, Lithium intercalation into bilayer graphene, Nat. Commun. **10**, 275 (2019).